International Journal of Heat and Mass Transfer 150 (2020) 119279

Contents lists available at ScienceDirect

International Journal of Heat and Mass Transfer

journal homepage: www.elsevier.com/locate/hmt

An explicit expression of the empirical factor in a widely used phase change model

Guang Chen, Taotao Nie, Xiaohong Yan*

Shaanxi Key Laboratory of Energy Chemical Process Intensification, Department of Chemical Engineering, Xi'an Jiaotong University, Xi'an, Shaanxi, 710049, China

ARTICLE INFO

Article history:
Received 7 March 2019
Revised 29 October 2019
Accepted 25 December 2019

Keyword:
Phase change
Lee model
Mass transfer
Boiling

ABSTRACT

Many boiling problems have been simulated by a phase change model (Lee model) involving an empirical mass transfer intensity factor. It is challenge to determine the value of this factor. An explicit expression of the mass transfer intensity factor is derived, and the accuracy of the expression is validated by comparing simulation results with theoretical solutions for two benchmark problems. The influences of various fluid properties (liquid phase density and thermal conductivity, latent heat, saturation temperature, vapor phase density and thermal conductivity) and mesh size on the mass transfer intensity factor are discussed. Results demonstrate that the mass transfer intensity factor depends on density and thermal conductivity of liquid phase, latent heat, saturation temperature and mesh size, but is independent of the density and thermal conductivity of vapor phase. Effects of vapor density and thermal conductivity on the phase interface movement are taken into account by the temperature of the interfacial cell. The expression reveals that a constant value of the mass transfer intensity factor throughout the computational domain is not reasonable, and which is the reason for divergence issue. In a specific computational cell, the value of the mass transfer intensity factor depends on the volume fraction of the liquid phase, and extremely large value of the factor should be consistent with extremely small volume fraction of the liquid phase.

1. Introduction

Boiling phenomenon can be observed in various industrial applications. However, the boiling process is very difficult to be predicted due to the complex heat and mass transfer process and the deformation of the vapor-liquid interface. The complexity of the actual boiling process limits the application of theoretical methods. Theoretical solutions are available for limited one-dimensional or two-dimensional problems. Numerical simulation is an efficient method to study the boiling process and to guide the design and optimization of related equipment. Details of mass and heat transfer behavior and the evolution of vapor-liquid interface can be obtained directly by numerical simulation. Furthermore, the numerical simulation is economical and convenient.

Various simulation methods have been developed for the capture of multiphase interface, such as the volume-of-fluid (VOF) method [1,2] and the level-set (LS) method [3,4]. Several phase change models have been proposed to calculate the heat and mass transfer across the phase interface, such as the Lee model [5], energy jump model or related modified models [6–12], the Schrage model or related modified models [13–14] and some new models [15–17]. These models are reviewed by Kharangate and Mudawar [18]. All these models can be used to evaluate the mass flux at the interface and source terms of the continuity equation and the energy equation. In the energy jump model and modified models [6–12], the mass flux at the interface is the function of the temperature gradient along the normal direction of the interface. It is difficult to determine the orientation of the interface and the temperature gradient along the normal direction of the interface. The common feature of such models [6–12] is that the temperature gradient calculation in the numerical frame involves temperature values for several cells neighbor to the interfacial cell. In the Schrage model, the mass flux is the function of an empirical factor and the interface temperature. On two sides of the interface, the saturation temperature values are assumed to be different in this model. Some modified models based on the Schrage model [14] provide mass flux expressions as a function of an empirical factor and the deviation between the interfacial cell temperature and the saturation temperature, which is similar to the Lee model. Recently, some new models [15–17] have been proposed. Pan et al.

* Corresponding author. Department of Chemical Engineering, Xi'an Jiaotong University, Xianning West Road #28, Xi'an, 710049, China.
E-mail address: xhyan11@mail.xjtu.edu.cn (X. Yan).

https://doi.org/10.1016/j.ijheatmasstransfer.2019.119279
0017-9310/

[15] proposed a model with a mass flux expression as the function of the time interval and the deviation between the interfacial cell temperature and the saturation temperature. The combination of interface capture method and the phase change model can be used to simulate the boiling process.

Among these phase change models, Lee model is the simplest one to be implemented with commercial computational fluid dynamics (CFD) software, which is also the widely used one. In the Lee model, the phase change rate is proportional to the deviation between the interfacial temperature and the saturation temperature, and only the temperature and phase volume fraction of the interfacial cell are required. The Lee model allows the phase change to occur at exist phase interface or within the saturated phase without phase interface initially, which means that the Lee model is able to simulate the boiling process without a predetermined phase interface and is suitable for the simulation of subcooled boiling problem. In addition, the convergence of the simulation can be guaranteed by adjusting an empirical factor.

However, there is an empirical factor in the Lee model, which is called as *mass transfer intensity factor* and denoted as r. Previous researches [19] demonstrated that small values of r cause a significant deviation between the interfacial temperature and the saturation temperature, but excessively large values of r cause numerical convergence problems and the optimal value of r must be found for each case by users, empirically. A wide range of this factor, from 0.1 to 5000 s^{-1} [20–24], has been reported in literature to simulate boiling problems. Wu et al. [20] investigated the refrigerant flow boiling in a horizontal serpentine tube with $r = 0.1$ s^{-1}. The same value of $r = 0.1$ s^{-1} was used by De Schepper et al. [21] and Alizadehdakhel et al. [22] in their simulation. Yang et al. [23] simulated the two-phase boiling flow in a coiled tube, and recommended a value of 100 s^{-1} in order to numerically maintain the interface temperature at $T_{sat} \pm 1$ K. Larger values of r were also used, such as 5000 s^{-1} in Gorle et al. [24].

Although the Lee model has been widely used, some questions are still open to be answered. Some of these questions are:

(1) Why the value of the empirical factor differs case by case, as reported in literature? What is the reason for the wide range of the mass transfer intensity factor (0.1 to 5000 s^{-1})?
(2) According to the source term expression in Lee model, the simulation results are accurate when the value of the empirical factor approaches infinite. However, in actual simulations, a finite value is used for a specific problem due to the divergence issue. Accordingly, the accuracy of the simulation results is unclear.
(3) In almost all simulation practices, the factor is used as a constant throughout the computational domain. Is it reasonable?

In this paper, an expression of the mass transfer intensity factor is derived. The accuracy of the expression is evaluated by simulating two benchmark problems: one-dimensional Stefan problem and the two-dimensional film boiling problem [17,25,26]. The detailed dependence of the mass transfer intensity factor on various fluid properties is discussed. Some open questions related with the mass transfer intensity factor are discussed.

2. Method

2.1. Governing equations

In this study, the simulation is based on the VOF method developed by Hirt and Nichols [1]. In the VOF method, the distribution of each phase and the shape of the phase interface are represented by the volume fraction α, which ranges from 0 to 1. In one computational cell, the value of 0 or 1 represents that this cell is empty or full with one specific phase. In each computational cell, the volume fractions of vapor phase and liquid phase sum to unity for boiling problems, that is

$$\alpha_v + \alpha_l = 1 \tag{1}$$

The tracking of the vapor-liquid interface is accomplished by solving the volume fraction equations. For the vapor phase, the volume fraction equation is

$$\frac{\partial}{\partial t}(\rho_v \alpha_v) + \nabla \cdot (\rho_v \alpha_v \mathbf{v}) = S_v \tag{2}$$

where α_v, ρ_v, $\mathbf{v}$ are the vapor volume fraction, vapor density, and the velocity field, respectively. S_v is the mass source term associated with the phase change. The volume fraction of the liquid phase is calculated according to Eq. (1).

In each cell, the physical properties of density ρ, thermal conductivity k and viscosity μ are determined as volume-fraction weighted average of liquid and vapor phases.

$$\rho = \alpha_l \rho_l + \alpha_v \rho_v \tag{3}$$

$$k = \alpha_l k_l + \alpha_v k_v \tag{4}$$

$$\mu = \alpha_l \mu_l + \alpha_v \mu_v \tag{5}$$

The vapor and liquid phases share a single momentum equation, and share the velocity field. The momentum equation is:

$$\frac{\partial}{\partial t}(\rho \mathbf{v}) + \nabla \cdot (\rho \mathbf{v}\mathbf{v}) = -\nabla p + \nabla \cdot \left[\mu\left(\nabla \mathbf{v} + \nabla \mathbf{v}^{\mathrm{T}}\right)\right] + \rho \mathbf{g} + \mathbf{F}_s \tag{6}$$

where p and $\mathbf{g}$ are the pressure field and the gravitational acceleration vector, respectively. F_s is the body force caused by the surface tension at the interface, which is calculated by the continuum surface force (CSF) model proposed by Brackbill et al. [27].

The energy equation is

$$\frac{\partial}{\partial t}(\rho E) + \nabla \cdot [\mathbf{v}(\rho E + p)] = \nabla \cdot [k \nabla T] + S_h \tag{7}$$

where S_h is the volumetric energy source. E is sensible enthalpy calculated by

$$E = C_p (T - T_{sat}) \tag{8}$$

where T_{sat} is the saturation temperature, and C_p is the specific heat capacity

$$C_p = \frac{\rho_v \alpha_v C_{p,v} + \rho_l \alpha_l C_{p,l}}{\rho_v \alpha_v + \rho_l \alpha_l} \tag{9}$$

where $C_{p,v}$, $C_{p,l}$ are the specific heat capacity for vapor and liquid phases, respectively.

2.2. Phase-change model——Lee model

In Lee model, the phase change is assumed to occur at a constant pressure and at a quasi-thermal equilibrium state. Moreover, the phase change is mainly dependent of the deviation of the interfacial cell temperature and saturation temperature T_{sat}, and an empirical multiplier is proposed to adjust the mass flux at interface. For boiling problem, the mass source term of the vapor volume fraction equation (Eq. (2)) is

$$S_v = r \alpha_l \rho_l \frac{T - T_{sat}}{T_{sat}} \quad (T > T_{sat}) \tag{10}$$

where r is the empirical mass transfer intensity factor, with a unit of s^{-1}. The value of r is recommended to maintain the interfacial temperature reasonably close to T_{sat}, and to avoid numerical divergence problem. The energy source term in the energy equation (Eq. (7)) is to release the heat caused by the mass transfer, which is the product of the negative mass source and the latent heat per mass ($S_h = -S_v h_{lv}$).

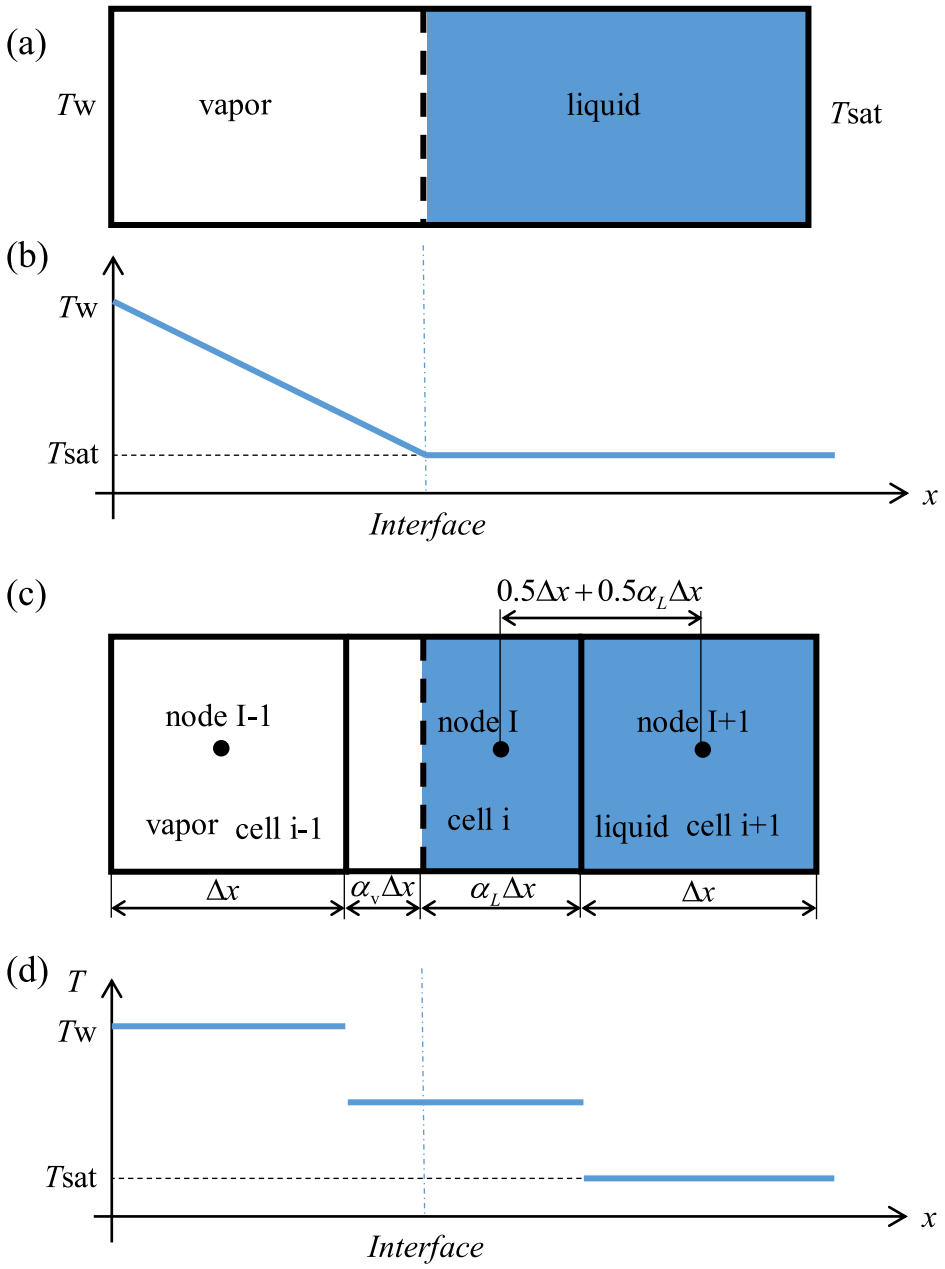

Fig. 1. Theoretical and numerical descriptions of the phase change problem.

3. Derivation of the expression

Two assumptions are employed to derive the expression of the mass transfer intensify factor:

(1) There is a liquid cell neighbor to the interfacial cell, and the temperature of the liquid cell equals the saturation temperature during the phase change process.
(2) The conductive heat flux from the interfacial cell to the neighbor liquid cell is the driven force of the phase change process.

In this section, the physical process of a one-dimensional phase change problem is considered, as shown in Fig. 1(a). Heat transfers from a vapor film to the saturated liquid (T_{sat}). The temperature of the left side of the vapor film is a constant (T_w). The interface moves as time goes on. The movement of the interface is along a fixed direction, denoted as x-axis.

From theoretical aspect, heat transfers from the vapor phase to the interface. At a moment, the temperature distribution is schematically shown in Fig. 1(b). The temperature of the interface equals the saturation temperature at any moment.

From numerical aspect, the computational domain is discretized into several cells or meshes, as shown in Fig. 1(c). For a physical variable, such as the temperature, a uniform distribution in a cell is assumed. Accordingly, the distribution of a physical variable in the computational domain is discontinuous, as shown in Fig. 1(d). Three cells are shown in Fig. 1(c), and they are denoted as i-1, i, $i + 1$. Three nodes are also shown in the figure, and they are denoted as I-1, I, $I + 1$. Cell i contains a phase interface, and this cell is called the interfacial cell. Heat transfers from the vapor cell i-1 to the interfacial cell i. In the interfacial cell, the domain is divided into the vapor subdomain and the liquid subdomain occupied by vapor phase and liquid phase, respectively. Node I locates in the middle position of the liquid subdomain. Node $I + 1$ is in the mid-

dle position of the cell $i + 1$. In the interfacial cell, the temperature is represented by one value. Hence, the temperature of node I is approximated as the cell temperature, which is known for a specific simulation. That is

$$T_{\mathrm{I}} = T_{\mathrm{i}} \tag{11}$$

In actual numerical simulation, the temperature of cell $i + 1$ may be larger than the saturation temperature, such as the results of Lee model (will discussed later according to simulation results). Reasonable phase change model should provide results being consistent with the theoretical situation. Theoretically, the temperature of cell $i + 1$ should equal the saturation temperature. Hence, the following condition is applied to force the simulation results to be consistent with the theoretical situation,

$$T_{\mathrm{I+1}} = T_{\mathrm{sat}} \tag{12}$$

Hence, the heat flux from the node I to the node $I + 1$ can be evaluated by first-order difference,

$$q = k_l \cdot \frac{T - T_{\mathrm{sat}}}{0.5\Delta x + 0.5\alpha_l \Delta x} \tag{13}$$

According to the assumptions in this section, this heat flux should be converted into latent heat so that the temperature of cell $i + 1$ and node $I + 1$ remains the saturation temperature.

Accordingly, the mass flux for phase change is

$$m = \frac{q}{h_{lv}} = k_l \cdot \frac{T - T_{sat}}{0.5\Delta x + 0.5\alpha_l \Delta x} \cdot \frac{1}{h_{lv}} \tag{14}$$

This mass flux is converted into the body source of the volume fraction equation as

$$S_{\mathrm{v}} = m \cdot \frac{\mathrm{A_{int}}}{\mathrm{V}} = k_l \cdot \frac{T - T_{sat}}{h_{lv}(0.5 + 0.5\alpha_l)\Delta x} \frac{\mathrm{A_{int}}}{\mathrm{V}} \tag{15}$$

This source expression is derived based on a one-dimensional problem. However, it is also expected to provide reasonable prediction accuracy for two-dimensional or three-dimensional problems. For two-dimensional or three-dimensional problems, the interface orientation in the interfacial cell may be not parallel to the axis. The physical meaning of the heat flux (Eq. (13)) or mass flux (Eq. (14)) for this situation is the flux along the normal direction of the interface. The application of current model forces the liquid temperature to be the saturation temperature for a point away from the interfacial cell with a distance of $(0.5\Delta x + 0.5\alpha_l \Delta x)$ along the normal direction. In the following section, a two-dimensional problem with a complex interface shape will be tested to check the accuracy of current model.

The mass source expression of current derivation has the similar configuration as the Lee model. Eq. (15) can be rewritten as

$$S_{\mathrm{v}} = \frac{T_{sat}}{h_{lv}(0.5 + 0.5\alpha_l)\Delta x \cdot \alpha_l \rho_l / k_l} \frac{\mathrm{A_{int}}}{\mathrm{V}} \cdot \frac{\alpha_l \rho_l (T - T_{sat})}{T_{sat}} \tag{16}$$

By comparing with the mass source expression in Lee model, the empirical mass transfer intensity factor can be expressed as

$$r = \frac{1}{\frac{(0.5+0.5\alpha_l)\Delta x}{k_l/(\rho_l C_{p,l}\alpha_l)} \cdot \frac{h_{lv}}{C_{p,l} T_{sat}}} \frac{\mathrm{A_{int}}}{\mathrm{V}} \tag{17}$$

In the expression, Δx denotes the characteristic size of the mesh. k_{l}, ρ_{l} and C_{pl} denote the thermal conductivity, density, specific heat capacity of the liquid phase, respectively. h_{lv} is the latent heat coefficient. α_{l} is the liquid phase volume fraction in the interfacial cell. Values of all these parameters can be obtained for a specific simulation problem. Thus, the mass transfer intensity factor can be calculated by this explicit expression without empirical guess.

The ratio of the interfacial area to the cell volume (A_{int}/V) can be evaluated according to the following expression,

$$\frac{\mathrm{A_{int}}}{\mathrm{V}} = |\nabla \alpha_{\mathrm{v}}| \tag{18}$$

For simplicity, A_{int}/V is approximated as $1/\Delta x$ in current simulation. More accurate simulation should use Eq. (18).

In the following section, two benchmark problems are simulated by this expression of mass transfer intensity factor and the sensitivity of various parameters on the expression is evaluated.

4. Results and discussion

4.1. One-dimensional Stefan problem

4.1.1. Problem description

The one-dimensional Stefan problem is simulated in a two-dimensional region by ANSYS Fluent 17.2, as shown in Fig. 2. The phase change model is realized by user defined functions. The heat transfer and interface movement occur along the x-axis. Free-slip and adiabatic conditions are applied at the top and bottom boundaries. Thus, no gradients exist along the y-axis, which guarantees the comparability between the simulation results and the one-dimensional theoretical solutions.

Initially, a thin vapor film attaches the wall with constant temperature T_{w}. The wall temperature is 10 K larger than the saturation temperature. Saturated liquid attaches the vapor film. In this simulation, the vapor film thickness is the length of the first mesh attached the wall. The length of the computational domain is 1 mm. A no-slip condition and a given pressure condition are provided at the boundaries of x equaling 0 mm and 1 mm, respectively. When time goes on, heat transfers from the wall to the vapor film and the phase interface. Accordingly, liquid phase changes to vapor phase and the interface moves along the x-axis.

The analytical solutions for the interface position $x(t)$ and the temperature $T(x,t)$ are given by:

$$x(t) = 2\beta\sqrt{\frac{k_v t}{\rho_v c_{p,v}}} \tag{19}$$

$$T(x,t) = T_{wall} + \left(\frac{T_{sat} - T_{wall}}{erf(\beta)}\right) erf\left(\frac{x}{2\sqrt{t \cdot k_v/\rho_v c_{p,v}}}\right) \tag{20}$$

where $erf(x)$ is the error function, and β is the solution of the transcendental equation

$$\beta \exp\left(\beta^2\right) erf(\beta) = \frac{c_{p,v}(T_w - T_{sat})}{h_{lv}\sqrt{\pi}} \tag{21}$$

4.1.2. Comparison with theoretical solutions

Water and steam at a system pressure of 101.3 kPa are considered as fluid in the Stefan problem. The physical properties are shown in Table 1.

As described in the above section, vapor exists in the first mesh attached the wall, initially. That is, the film thickness is the length of the first mesh. According to the theoretical solution of the interface location, the time required for vapor film to develop a given thickness can be calculated. Three mesh configurations with uniform sizes of 2 μm, 5 μm, 10 μm are tested to evaluate the mesh sensitivity on the simulation results. For such three mesh configurations, the times required for developing a vapor film thickness of 2 μm, 5 μm, 10 μm are 1.08 $\times$ $10^{-}5$ s, 6.75 $\times$ $10^{-}5$ s and 2.7 $\times$ $10^{-}5$ s respectively. These time values are set as the initial computational time, being consistent with the initial vapor film thickness. Initially, a linear temperature distribution is applied in the vapor film between the wall temperature T_{W} and the saturation temperature T_{sat}.

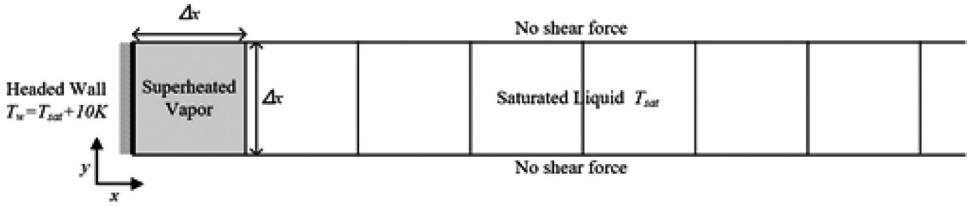

Fig. 2. Schematic description of the Stefan problem with boundary conditions.

Table 1
Properties of water and water vapor at 101.3 *kPa*.

	Density $\rho(kg/m^3)$	Viscosity $\mu(kg/m \cdot s)$	Heat capacity $C_p(J/kg \cdot K)$	Thermal conductivity $k(W/m \cdot K)$	Latent heat $h_{lv}(J/kg)$	Surface tension $\sigma_{lv}(N/m)$
Vapor	0.597	1.26×10^{-5}	2030	0.025	2.26×10^{6}	0.059
Liquid	958.4	2.8×10^{-4}	4216	0.679		

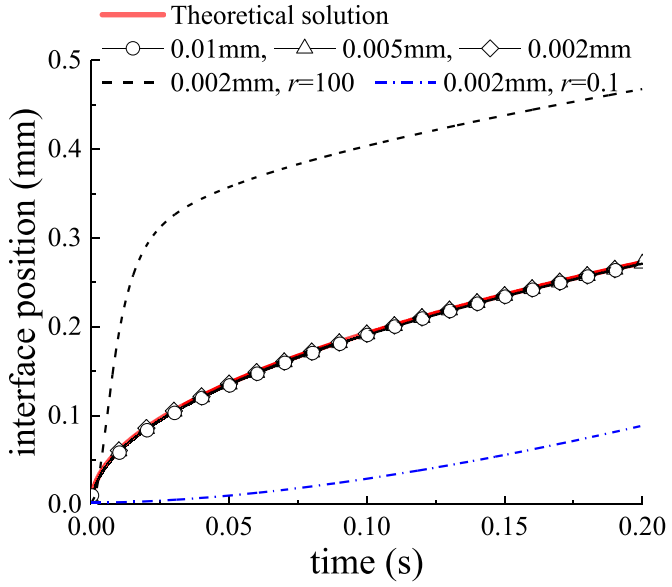

Fig. 3. Comparison of theoretical and numerical interface positions as a function of time.

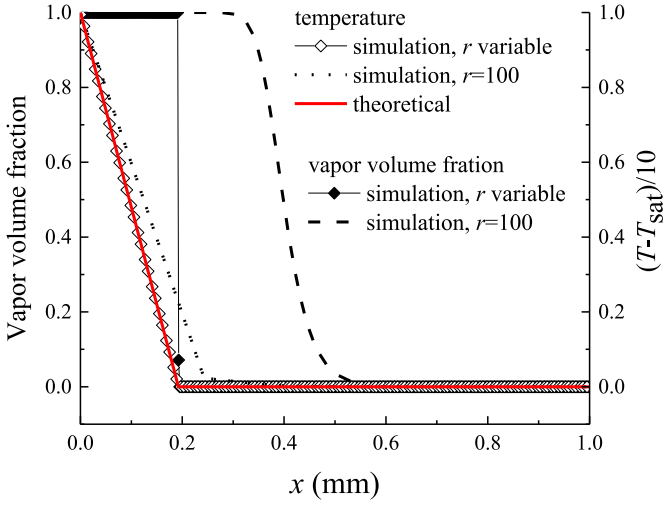

Fig. 4. The vapor volume fraction and temperature along the *x*-axis at the moment of 0.1 s. The mesh size is 2 μm.

The theoretical solution of the interface location as a function of time is shown in Fig. 3 (red line). The same problem is simulated by the Lee model. The value of the mass transfer intensity factor corresponding to the interfacial cell in the computational domain is calculated by current expression in Eq. (17). In cells other than the interfacial cell, the mass source and energy source terms are zero. Three different mesh configurations (uniform mesh size of 2 μm, 5 μm, 10 μm) are test. The simulation results are shown in Fig. 3 (lines with symbols). As shown in the figure, simulation results agree well with analytical solutions. The deviations among simulation results corresponding to three mesh configurations are small, indicates that the mesh size of 2 μm is fine enough to predict the interface movement (with the deviation 0.15%). When the mesh size of 2 μm is used, values of the mass transfer intensity factor in the computational domain is in the range of $(2.34 \times 10^4, \infty)$ s^{-1}. The values of 2.34×10^4 and ∞ correspond to two situations of the liquid volume fraction in an interfacial cell approaching 1.0 and 0.0, respectively. The vapor volume fraction and temperature along the axis are shown in Fig. 4 (lines with symbols). Theoretical solution of the temperature (Eq. (20)) is also shown for comparison (red line). Good agreement between the theoretical solution and the simulation with variable *r* calculated by current expression (line with open circle symbol) can be observed. One interfacial cell ($0 < \alpha_v < 1$) can be observed according to the simulation result (line with closed diamond symbol). The good agreement shows that it is possible to determine the empirical mass transfer intensity factor in Lee model without trial and error method.

In almost all simulations by the Lee model in literature, the mass transfer intensity factor in the whole computational domain for a specific problem is a const. Current expression (in Eq. (17)) reveals that constant value of the factor is not accurate. The value of the factor depends on the liquid volume fraction in the interfacial cell. Values of the liquid volume fraction in different interfacial cells are different and vary with time in the range of 0 to 1. Hence, in a specific computational domain with a given mesh configuration, the value of the mass transfer intensity factor varies with time and local position in the range of a finite value to the infinite value, such as $(2.34 \times 10^4, \infty)$ s^{-1} for current case.

Two widely used values of the factor (0.1 and 100) in open literature are also used in the Lee model, and the simulation results are shown in Fig. 3 for comparison (dash line and dash-dot line). Obvious deviation of interface location can be observed. As can be observed from Fig. 4 (dash line), there are various interfacial cells along the axis direction when *r* is 100, which is not physically reasonable. In addition, obvious deviation between the temperature distribution (dot line) and the theoretical solution (red solid line) can be observed. Hence, unreasonable value of the mass transfer intensity factor indeed results in inaccurate simulation results.

Table 2
Cases with various fluid properties.

Cases	ρ_L kg/m^3	k_L W/(m•K)	ρ_v kg/m^3	k_v W/(m•K)	h_{lv} J/kg	T_{sat} K	r s^{-1}
1	958.4	0.679	0.597	0.025	2.26×10^6	298.15	$(2.34 \times 10^4, \infty)$
2	500	0.679	0.597	0.025	2.26×10^6	298.15	$(4.48 \times 10^4, \infty)$
3	200	0.679	0.597	0.025	2.26×10^6	298.15	$(1.12 \times 10^5, \infty)$
4	958.4	0.3	0.597	0.025	2.26×10^6	298.15	$(1.03 \times 10^4, \infty)$
5	958.4	0.1	0.597	0.025	2.26×10^6	298.15	$(3.44 \times 10^3, \infty)$
6	958.4	0.679	0.597	0.025	3×10^6	298.15	$(1.76 \times 10^4, \infty)$
7	958.4	0.679	0.597	0.025	1×10^6	298.15	$(5.28 \times 10^4, \infty)$
8	958.4	0.679	0.597	0.025	2.26×10^6	373.15	$(2.92 \times 10^4, \infty)$
9	958.4	0.679	1	0.025	2.26×10^6	298.15	$(2.34 \times 10^4, \infty)$
10	958.4	0.679	2	0.025	2.26×10^6	298.15	$(2.34 \times 10^4, \infty)$
11	958.4	0.679	0.597	0.1	2.26×10^6	298.15	$(2.34 \times 10^4, \infty)$
12	958.4	0.679	0.597	0.679	2.26×10^6	298.15	$(2.34 \times 10^4, \infty)$

4.1.3. Dependence of the factor on various fluid properties

Many simulations in literature indicate that the mass transfer intensity factor varies from one problem to another problem, and even for a specific problem, the value of the factor may varies with the cell location [24]. However, detailed dependence of the factor on various parameters is unknown, which obstructs the application of the Lee model.

The expression (Eq. (17)) shows the dependence on various fluid properties. In order to evaluate the accuracy of the dependence, more cases with different fluid properties are simulated by the Lee model with current expression. The fluid properties for all cases are shown in Table 2. The simulation results are compared with analytical solutions, as shown in Fig. 5. Good agreements can be observed for all cases, which prove that the dependence of r on various fluid properties described by the expression is accurate. In addition, this agreement also demonstrates that different values of r should be applied for different problems. The ranges of r for various cases are shown in Table 2.

An interesting observation is described here. Note that expressions of r (Eq. (17)) and source term (Eq. (16)) are independent of the vapor phase density and thermal conductivity. However, the interface movement depends on these two fluid properties, as shown in the analytical solution (Eq. (19)). The good agreement between simulation results and analytical solutions indicates that r is indeed independent of the vapor phase density and thermal conductivity. Thus, the influence of the vapor phase density and thermal conductivity on the interface movement is realized by the temperature of the interfacial cell, which is included in the expression of source term.

In conclusion, the value of r depends on the liquid phase density and thermal conductivity, latent heat, saturation temperature and the liquid volume fraction in the interfacial cell, and is independent of the vapor phase density and thermal conductivity. In various actual boiling problems, the fluid material, pressure, temperature are different, hence the value of r should be consistent with such fluid properties.

4.1.4. Dependence of the factor on mesh size

Except fluid properties, the expression also shows the dependence of r on mesh size. In actual simulation of large scale problems, non-uniform mesh distribution in a computational domain is usually used. In order to evaluate the accuracy of current expression under this condition, a non-uniform mesh (range from 1 μm to 10.9 μm) is generated for the Stefan problem. This case is denoted as Case 13. Fine meshes are used in the region near the heat wall due to the large temperature gradient and coarse meshes are used in the region away from the heat wall. The total mesh number in the region of 1 mm is 241. Fig. 6 shows several meshes near the heat wall. The parameter Δx in the expression of r is calculated for each mesh. The simulation results are compared with the analytical solution, as shown in Fig. 7. A good agreement can be observed, which indicates the applicable of current expression in non-uniform mesh configuration.

Table 3
The properties of liquid and vapor for 2D film boiling problem.

	Density $\rho(kg/m^3)$	Viscosity $\mu(kg/m \cdot s)$	Heat capacity $C_p(J/kg \cdot K)$	Thermal conductivity $k(W/m \cdot K)$
Vapor	5	0.005	200	1
Liquid	200	0.1	400	40

4.2. Two-dimensional film boiling problem

4.2.1. Physical problem description

Fig. 8 shows the schematic of the two-dimensional axial symmetry film boiling problem. The bottom wall is superheated and covered by a layer of vapor, and above them are the saturated liquid. In this problem, the liquid and vapor phases are incompressible and have constant properties. These properties are given in Table 3. The latent heat per mass (h_{lv}), surface tension coefficient (σ), saturation temperature (T_{sat}) are 10 kJ/kg, 0.1 $N•m$, and 373.15 K, respectively. The gravity force is along the negative y-axis with the acceleration g of 9.81 m/s^2.

The width of the film is the "most dangerous" Taylor wavelength [28],

$$l_m = 2\pi \sqrt{\frac{3\sigma}{(\rho_l - \rho_v)g}} = 0.07868 \text{ m} \tag{22}$$

Because of the axis-symmetrical configuration, the width of the computational domain is $l_m/2$. The height of the computational domain is $3l_m/2$ to observe the whole bubble shape. The bottom wall is set as a no-slip boundary with a superheated temperature of 5 K. An axial-symmetry boundary and a free-slip boundary are used for the left and right boundaries, respectively. The top boundary is a pressure-outlet boundary.

Initially, the liquid is saturated, and a linear temperature distribution from the superheated wall to the liquid-vapor interface is applied in vapor layer. The initial interface shape is set according to the following equation

$$y(x, 0) = \frac{l_m}{128}\left[4.0 + \cos\left(\frac{2\pi x}{l_m}\right)\right] \tag{23}$$

4.2.2. Interface variation

Four mesh configurations are used to evaluate the mesh dependence on the simulation results, which are $40(x) \times 120(y)$, $60(x) \times 180(y)$, $80(x) \times 240(y)$ and $100(x) \times 300(y)$. Fig. 9 shows the ratio of the vapor volume fraction to the initial vapor volume fraction $\alpha_v/\alpha_{v,0}$ in a time interval. As shown in Fig. 9, the mesh

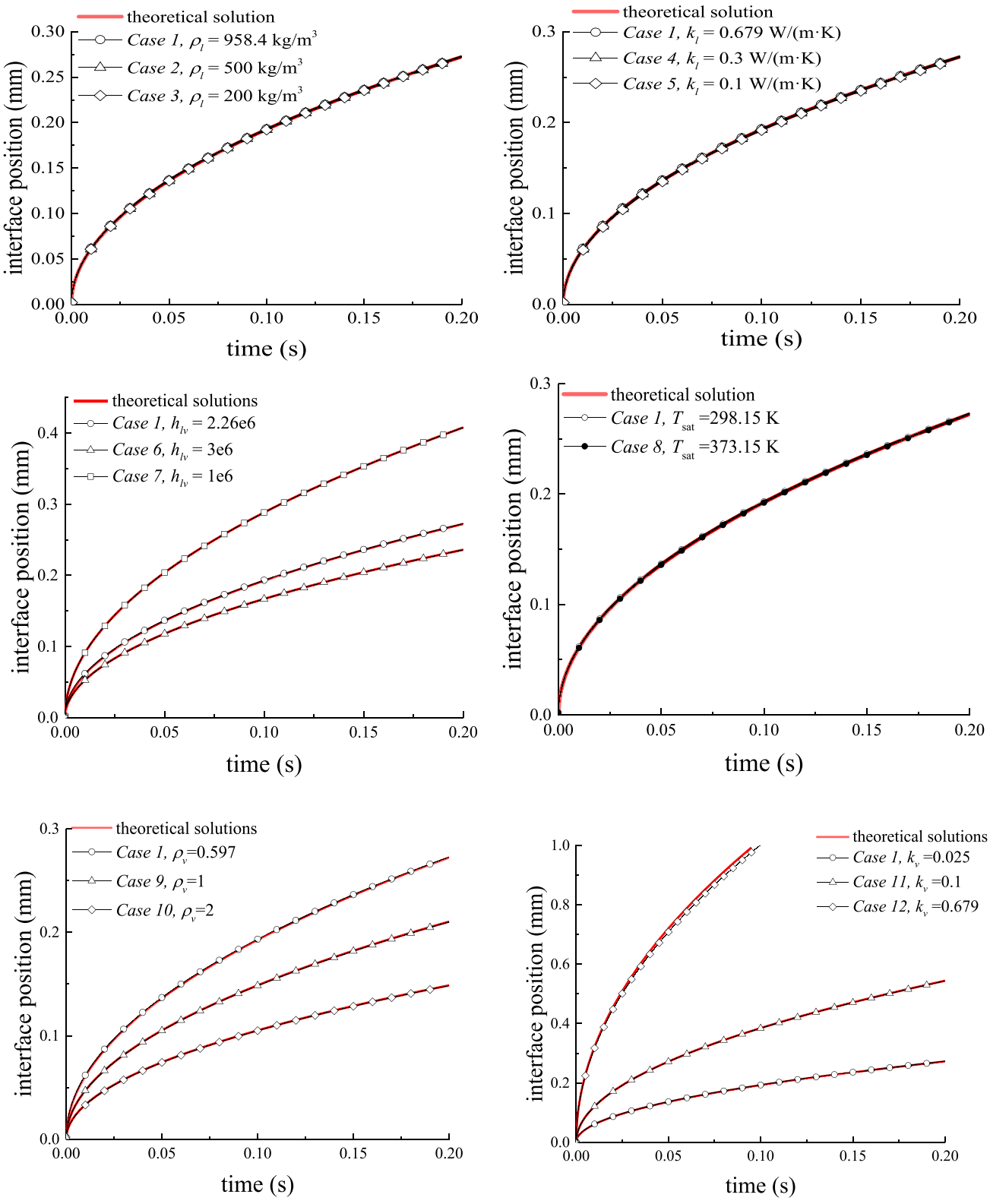

Fig. 5. Comparison of theoretical and numerical interface position of various 1D Stefan problems.

Fig. 6. Part of the non-uniform mesh size.

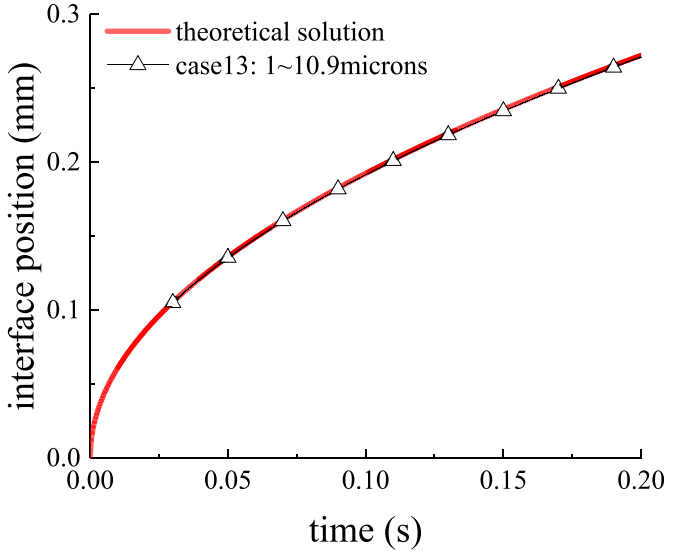

Fig. 7. Comparison of the interface positions between theoretical prediction and numerical simulation with a non-uniform mesh distribution.

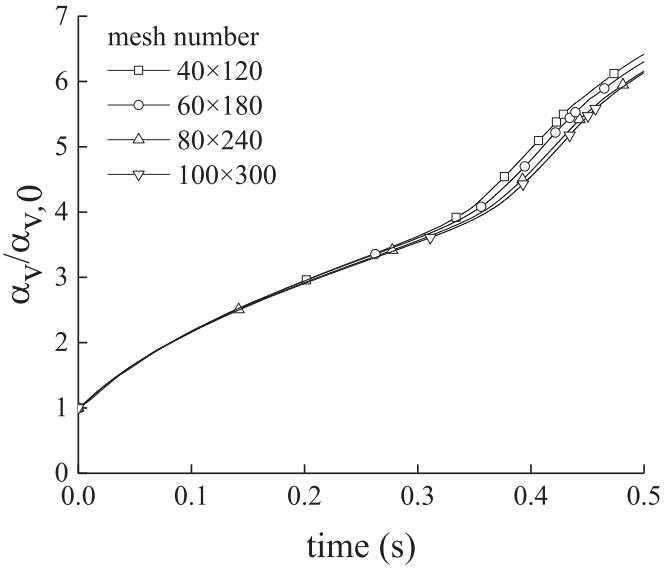

Fig. 9. Dependence of the vapor volume fraction on mesh configurations.

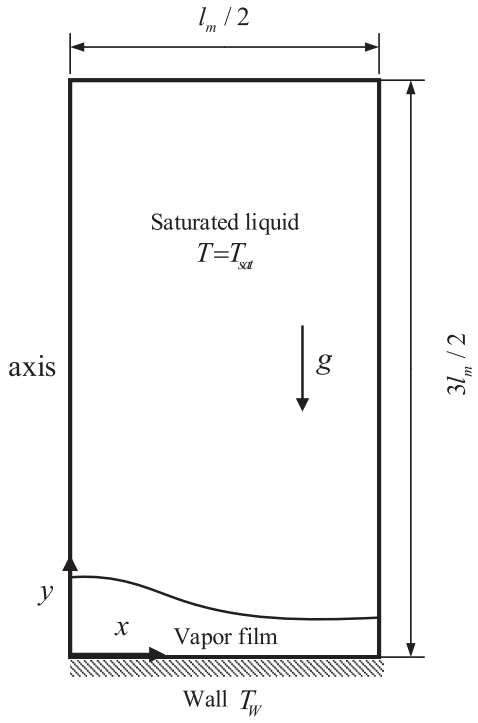

Fig. 8. Schematic of the two-dimensional film boiling problem.

configurations 80(x) × 240(y) and 100(x) × 300(y) provide nearly identical results, and the mesh configuration of 80(x) × 240(y) is used in the subsequent simulations.

Fig. 10 shows the liquid-vapor interface shapes at several moments. The thickness of the vapor film increases with time and a bubble gradually form and growth in the middle section. The bubble eventually reaches a limit and detaches from the vapor film. After the bubble detachment, the vapor film shrinks, and grows again to form the next bubble. Nearly periodic bubble growth and detachment processes can be observed and this periodic behavior is consistent with results reported in literature [17]. In order to evaluate the simulation accuracy, theoretical results of the heat transfer

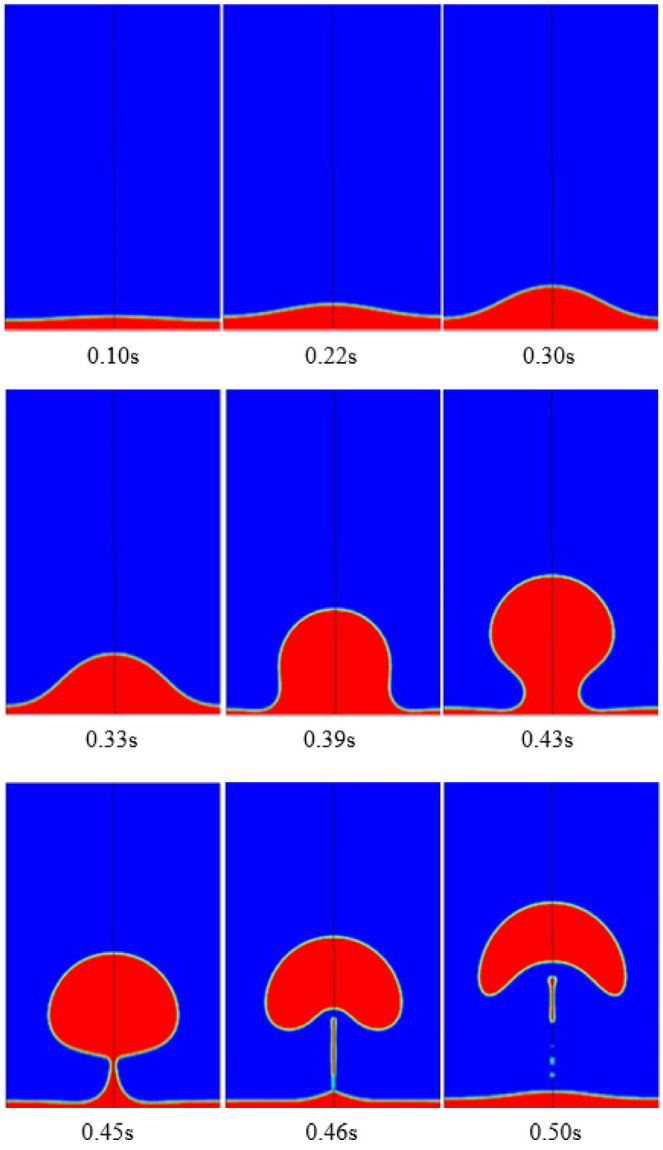

Fig. 10. Phase distributions at different moments for the two-dimensional film boiling problem.

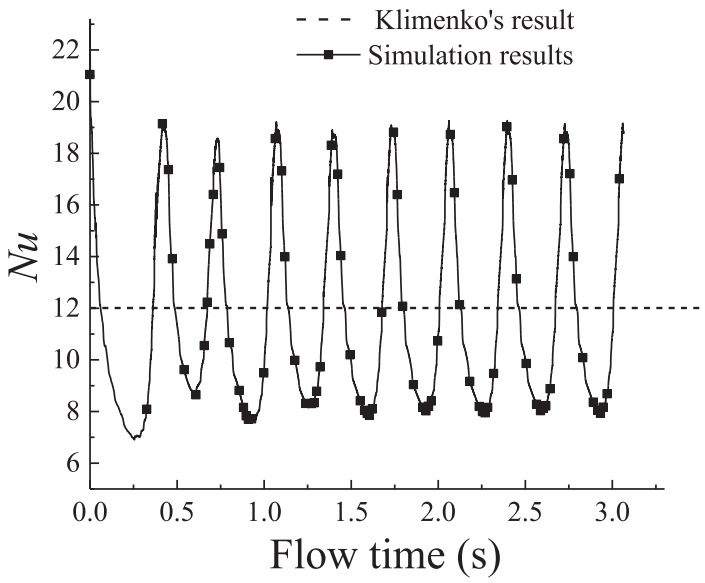

Fig. 11. Comparison of the Nusselt number for two-dimensional film boiling problem between theoretical solution and numerical simulation result.

characteristic of the film boiling problem are used for comparison in the following section.

4.2.3. Nusselt number

Klimenko [29] proposed several correlations to predict heat transfer characteristic of film boiling process on a horizontal surface. These correlations provide reasonable prediction accuracy of several experimental data with an accuracy of ±25%.

The expression of the Nusselt number for laminar vapor flow (which is the situation of current case) is:

$$Nu = 0.19[Ga(\rho_l/\rho_v - 1)]^{1/3}\Pr_v^{1/3} f_1, \quad Ga(\rho_l/\rho_v - 1) < 10^8 \quad \text{(Laminar)} \tag{24}$$

where

$$f_1 = \begin{cases} 1 & \frac{h_{lv}}{c_{p,v}(T_w - T_{sat})} \le 1.4 \\ 0.89\left[\frac{h_{lv}}{c_{p,v}(T_w - T_{sat})}\right]^{1/3} & \frac{h_{lv}}{c_{p,v}(T_w - T_{sat})} > 1.4 \end{cases} \tag{25}$$

In Eq. (24), Ga is the Galileo number, and Pr is the Prandtl number, and they are expressed as

$$Ga = \frac{g {l_{cr}}^3}{{\nu_v}^2} \tag{26}$$

$$Pr_v = \frac{\mu_v C_{p,v}}{k_v} \tag{27}$$

where l_{cr} is the critical wave length.

$$l_{cr} = 2\pi\sqrt{\frac{\sigma}{(\rho_l - \rho_v)g}} \tag{28}$$

According to these expressions, the Nusselt number for current case is 12.01. In our simulation, the Nusselt number is calculated as follows:

$$Nu = \frac{q_{avg,w}}{(T_w - T_{sat})}\frac{l_{cr}}{k_v} \tag{29}$$

where $q_{avg,w}$ is the area-weight average heat flux at the heated wall.

Fig. 11 shows the comparison of the Nusselt number between the theoretical result and the numerical result. Theoretical correlations provide the time-averaged value and the numerical simulation is capable of providing time-dependent value. As shown in the figure, simulation indicates that the Nusselt number varies periodically with time, being consistent with the periodic bubble formation and detachment behavior. The time-averaged Nusselt number according to the simulation result is 11.23, which demonstrates a reasonable agreement with the theoretical result with a deviation of 6.5%. The empirical factor r for this simulation ranges from 2.47×10^4 to ∞.

The reasonable bubble formation and detachment behavior and Nusselt number proves the ability of current expression to predict two-dimensional film boiling problem.

5. Conclusions

An expression of the mass transfer intensity factor in Lee model is derived. The accuracy of the expression is proved by simulating two benchmark problems: one-dimensional Stefan problem and two-dimensional film boiling problem. The expression provides a way to calculate the mass transfer intensity factor as a function of fluid properties and mesh size, without trial and error. The expression reveals that a constant value of the mass transfer intensity factor throughout the computational domain is not reasonable and may cause the divergence issue. The value should be a function of the volume fraction of liquid phase in the interfacial cell. In addition, the expression explicitly shows the dependence of the mass transfer intensity factor on various fluid properties and mesh size. This dependence provides the reason for the scatter of the mass transfer intensity factor reported in literature.

The Lee model is the simplest model for large-scale phase change problems, and current expression can be combined with the Lee model to provide more accurate results without empirical factor. More complex boiling problem will be simulated in the future.

Declaration of Competing Interest

The authors declare that there are no conflicts of interest.

Acknowledgments

The authors greatly acknowledge the financial supports from the Natural Science Foundation of China (No. 51576157) and the Fundamental Research Funds for the Central Universities.

References

[1] C.W. Hirt, B.D. Nichols, Volume of fluid (VOF) method for the dynamics of free boundaries, J. Comput. Phys. 39 (1981) 201–225.
[2] S.W.J. Welch, J. Wilson, A volume of fluid based method for fluid flows with phase change, J. Comput. Phys. 160 (2000) 662–682.
[3] M. Sussman, P. Smereka, S. Osher, A level set approach for computing solutions to incompressible two-phase flows, J. Comput. Phys. 114 (1994) 146–159.
[4] G. Son, V.K. Dhir, Numerical simulation of film boiling near critical pressures with a level-set method, J. Heat Transf. – Trans. ASME 120 (1998) 183–192.
[5] W.H. Lee, A pressure iteration scheme for two-phase flow modeling, in: T.N. Veziroglu (Ed.), Multiphase Transport Fundamentals, Reactor Safety, Applications, 1, Hemisphere Publishing, Washington, DC, 1980.
[6] S. Shin, D. Juric, Modeling three-dimensional multiphase flow using a level contour reconstruction method for front tracking without connectivity, J. Comput. Phys. 180 (2002) 427–470.
[7] B.A. Nichita, J.R. Thome, A level set method and a heat transfer model implemented into fluent for modeling of microscale two phase flows, AVT-178 Specialists' Meeting on System Level Thermal Management for Enhanced Platform Efficiency, 2010.
[8] D.L. Sun, J.L. Xu, L. Wang, Development of a vapor-liquid phase change model for volume-of-fluid method in fluent, Int. Commun. Heat Mass Transf. 39 (8) (2012) 1101–1106.
[9] J. Xu Sun, Q. Chen, Modeling of the evaporation and condensation phase-change problems with fluent, Numer. Heat Transf. B 66 (2014) 326–342.
[10] I. Perez-Raya, S.G. Kandlikar, Numerical modeling of interfacial heat and mass transport phenomena during a phase change using ANSYS-Fluent, Numer. Heat Transf. Part B-Fundam. 70 (4) (2016) 322–339.
[11] Y.-Y. Tsui, S.-W. Lin, Y.-N. Lai, F.-C. Wu, Phase change calculations for film boiling flows, Int. J. Heat Mass Transf. 70 (2014) 745–757.
[12] Y. Sato, B. Niceno, A sharp-interface phase change model for a mass conservative interface tracking method, J. Comput. Phys. 249 (2013) 127–161.
[13] R.W. Schrage, A Theoretical Study of Interphase Mass Transfer, Columbia University Press, New York, 1953.
[14] I. Tanasawa, Advances in condensation heat transfer, in: J.P. Hartnett, T.F. Irvine (Eds.), Advances in Heat Transfer, Academic Press, San Diego, 1991.
[15] Z. Pan, J.A. Weibel, S.V. Garimella, A saturated-interface-volume phase change model for simulating flow boiling, Int. J. Heat Mass Transf. 93 (2016) 945–956.
[16] A.S. Rattner, S. Garimella, Simple mechanistically consistent formulation for volume-of-fluid based computations of condensing flows, J. Heat Transf 136 (071501) (2014) 1–9.
[17] S.T. Ding, B. Luo, G. Li, A volume of fluid based method for vapor-liquid phase change simulation with numerical oscillation suppression, Int. J. Heat Mass Transf. 110 (2017) 348–359.
[18] C.R. Kharangate, I. Mudawar, Review of computational studies on boiling and condensation, Int. J. Heat Mass Transf. 108 (2017) 1164–1196.
[19] D.G. Kim, C.H. Jeon, I.S. Park, Comparison of numerical phase-change models through Stefan vaporizing problem, Int. Commun. Heat Mass Transf. 87 (2017) 228–236.
[20] H.L. Wu, X.F. Peng, P. Ye, Y. Gong, Simulation of refrigerant flow boiling in serpentine tubes, Int. J. Heat Mass Transf. 50 (2007) 1186–1195.
[21] S.C.K. De Schepper, G.J. Heynderichx, G.B. Marin, Modeling the evaporation of a hydrocarbon feedstock in the convection section of a steam cracker, Comp. Chem. Eng. 33 (2009) 122–132.
[22] A. Alizadehdakhel, M. Rahimi, A.A. Alsairafi, CFD modeling of flow and heat transfer in a thermosyphon, Int. Commun. Heat Mass Transf. 37 (2010) 312–318.
[23] Z. Yang, X.F. Peng, P. Ye, Numerical and experimental investigation of two phase flow during boiling in a coiled tube, Int. J. Heat Mass Transf. 51 (2008) 1003–1016.
[24] C. Gorlé, P. Parida, H. Lee, F. Houdhmand, M. Asheghi, K. Goodson, Validation study for VOF simulations of boiling in a microchannel, ASME InterPACK, 2015–48129, 2015.
[25] D.K. Agarwal, S.W.J. Welch, G. Biswas, F. Durst, Planar simulation of bubble growth in film boiling in near-critical water using a variant of the VOF method, J. Heat Transf. (ASME) 126 (2004) 329–338.
[26] F. Gibou, L. Chen, D. Nguyen, S. Banerjee, A level set based sharp interface method for the multiphase incompressible Navier-Stokes equations with phase change, J. Comput. Phys. 222 (2007) 536–555.
[27] J.U. Brackbill, D.B. Kothe, C. Zemach, A continuum method for modeling surface tension, J. Comput. Phys. 100 (1992) 335–354.
[28] P.J. Berenson, Film-boiling heat transfer from a horizontal surface, J. Heat Transf. – Trans. ASME 83 (1961) 351–356.
[29] V.V. Klimenko, Film boiling on a horizontal plate—new correlation, Int. J. Heat Mass Transf. 24 (1981) 69–79.